Harmonic Suppression in Frequency Shifted Backscatter Communications

Yuan Ding, *Member, IEEE,* Romwald Lihakanga, Ricardo Correia, *Member, IEEE,* George Goussetis, *Senior Member, IEEE,* Nuno Borges Carvalho, *Fellow, IEEE*

Abstract This paper provides a comprehensive study of the harmonics generated by a frequency shifted backscatter communication system. The suppression and the manipulability of different harmonics are of importance to avoid detrimental inter-user interference when a number of backscattering nodes (and perhaps also other active wireless users) operate simultaneously in a network. In this paper the harmonics generated by a widely adopted open-short backscatter tag architecture is firstly presented. Then the ideal backscatter system which generates no unwanted harmonics is discussed, which inspires various harmonic suppression strategies. In particular, practical constraints of the backscatter tag hardware capabilities are applied, e.g. the number of discrete reflection coefficients that can be synthesized, and the dimension of the reflection coefficients (real-valued or complex-valued). Furthermore, the dual-transistor based IQ backscatter modulator is found useful to suppress all mirror harmonics and any specified higher order harmonics. The applicability of these proposed harmonic suppression approaches are demonstrated by an exemplar backscatter network consisting of multiple nodes performing binary frequency shifted keying (2FSK) modulated backscatter communications simultaneously.

Index Terms—Backscatter communications, harmonic suppression, reflection coefficient, spectrum sharing

I. INTRODUCTION

MASSIVE machine-type communications (MTC), as one of three important pillars to the ever-evolving 5G and beyond, have been gaining momentum to become an indispensable part of our everyday life [1]. The rise of the Internet of Things (IoT) networks is endowing intelligence to the world around us, fostering the concepts like Smart Home, Smart Factory, and Smart City [2]. The protocols and physical-layers have been purposely designed for IoT to construct the so-called Low-Power Wide-Area Networks (LPWANs), such as the widely deployed Narrowband-IoT (NB-IoT) and Long Range Wide-Area Networks (LoRaWAN). Featuring very narrow frequency bandwidth, those networks are able to reduce the power consumption down to the order of tens of mW, e.g. NB-IoT consumes 20~40 mW [SODAQ Mbili ATmega 1284P]. This low-

life of handheld devices, e.g mobile phones, wherein the energy is dominantly consumed on cellular connections, e.g. LTE handsets can radiate at a maximum of 500 mW. However, when considering the massive nodes in various types of wireless sensor networks (WSNs), a typical button battery can only support the continuous operation of the node for hours. Even in highly duty-cycled operations, the lifetime of a battery can hardly be extended to months. This brings challenges of unaffordable maintenance cost, e.g. replacing hundreds or thousands of batteries regularly (in some applications even this is inapplicable as nodes can be inaccessible), and environmental cost, e.g. the carbon emission associated with battery fabrication and toxic battery waste pollution [3]. This demand calls for new types of communication technologies that reside in the ultra-low-power regime, say three orders lower down to tens of μW, which in turn can be supported by harvested wireless [...] ached if the current active [...] aced with the passive backscatter transmissions [4], removing the needs of power-hungry radio frequency (RF) carrier synthesizers and power amplifiers. The sources of the wireless energy for powering the backscattering nodes can be the purposely designed power base-station/beacons [5], the Simultaneous Wireless Information and Power Transfer (SWIPT) transmitters [6], and even ambient commodity wireless networks [7] [8]. The powering strategy and the RF energy harvesting process are commonly associated with the downlink (power and information) in the networks, which is different to the

Yuan Ding, Romwald Lihakanga, and George Goussetis are with School of Engineering and Physical Sciences, Heriot-Watt University, Edinburgh EH14 4AS, Scotland, UK (e-mail: yuan.ding@hw.ac.uk; rkl2@hw.ac.uk; G.Goussetis@hw.ac.uk)

Ricardo Correia and Nuno Borges Carvalho are with Instituto de Telecomunicações, Departamento de Eletrónica, Telecomunicações e Informática, Universidade de Aveiro, Aveiro 3810-193, Portugal (e-mail: rjoao@ua.pt; nbcarvalho@ua.pt)

focus of this paper, i.e. the harmonic suppression techniques for the backscatter uplinks.

The backscatter technology was first utilized for Radar during the WWII. In a Radar system, a target object featuring a unique Radar Cross-Section (RCS) characteristic scatters the purposely generated high power illuminating electromagnetic waves in the backward direction (namely backscatter). By detecting and processing the scattered signals, the target information, e.g. distance, speed, etc., can be extracted. Later, by embedding unique codes into the backscattered signals, the Radio-frequency identification (RFID) technology was developed, which has been widely adopted in many scenarios, e.g. for logistic and sensing applications [9], [10].

Now, the trend of using backscatter technology for wireless communications has become irresistible due to its low-power and low-cost, allowing for massive deployment to fulfil the ambitious 'Smart Dust' [11] mission envisioned two decades ago. Enormous efforts have been witnessed to address some challenges facing (semi-)passive backscatter links. For example, compared with the conventional Ultra High Frequency (UHF) RFID links of up to a few meters, the communication range of the state-of-the-art backscatter communication systems has been extended to hundreds, and even thousands of meters, thanks to noise-resilient modulation schemes [12]–[14], extra array beamforming gains [15], and active gains obtained from tunnelling effect [16]. On the other frontline, higher order modulation schemes have been successfully implemented to improve the link data rates [17], [18], with a recent extension to multicarrier, e.g. orthogonal frequency-division multi-plexing (OFDM) waveforms, reported in [19]. The hardware architecture of backscatter tags has also witnessed great development in order to support diverse backscatter modulation waveforms. In particular, the conventional two-load switching solution [20] was extended to multiple-loads to support higher order modulations [21] [22]. When the switching frequency is linearly varied via a Voltage-Controlled Oscillator (VCO), the LoRa compatible chirp signals can be synthesized [23]. Apart from the switching solutions, the backscatter tags that are capable of continuously changing their impedances were constructed using PIN diodes and transistors [24], which opens the possibility of backscatter signal pulse shaping.

Aforementioned advancements have greatly improved the performance, with regard to the link budgets and data rates, of each individual backscatter link. However, a major challenge still exists when integrating a large number of them into a network, where the limited spectrum resources have to be efficiently shared, and the inter-user interference has to be effectively suppressed and managed [24]. Most previous backscatter works only pay attention to the in-band backscatter signals, leaving the harmonics un-treated [25]. As a consequence, when harmonics of one user fall into frequency bands allocated to other users that are required to operate simultaneously, the link performance of other users can be greatly compromised. This issue was first raised in [26], where a series of four discrete complex impedances was used to cancel out the first mirror harmonic. This was later extended to 8 discrete complex impedances for the 3rd and 5th order harmonic suppression [23]. These reported methods, however, are hardware-specific and are not scalable, i.e. cannot be adopted to suppress any specified harmonic components required by the network. The challenge and the limitations of the previous solutions motivate a comprehensive study of harmonic suppression methods in order to optimize the usage of backscatter network spectrum resources.

The contributions of this paper are now summarized as below:

- The ideal frequency shifted backscatter link with no harmonics generated is mathematically introduced, which needs to be supported by tags that can continuously vary their impedance along a complete reflection coefficient circle (Section III);
- The harmonics produced by the backscatter tags with discrete complex-valued reflection coefficients are investigated, and the results can guide harmonic suppression designs in the network. In addition, it is found that the methods described in [23] and [26] are special cases and non-optimal (Section III);
- It is revealed that any specified higher order harmonics can be purposely removed by carefully designing the real-valued (continuous and discrete) reflection coefficients-based backscatter tags (Section IV);
- The IQ backscatter modulator tag architecture is found useful in removing all mirror harmonic components (Section V);
- The applicability of various harmonic suppression approaches is demonstrated by exemplar systems comprising multiple backscatter nodes. The simulation results provide the insights about the trade-off between network performance and backscatter tag hardware complexity (Section VI).

II. Harmonics in Conventional Frequency Shifted Backscatter Systems

Amplitude shifted keying (ASK) modulation is adopted in the commercial UHF RFID systems, wherein a sophisticated reader is required to extract the weak backscatter signals out of the strong carrier waves that occupy a same frequency band. The strong in-band interference limits the performance of the ASK backscatter communication links. By shifting the backscatter signals away from the ambient signals in the frequency domain, the interference caused by ambient RF carriers is drastically reduced, thereby greatly improving the backscatter link budget [8], [9]. However, beyond backscattering the signal at the desired frequency band, this approach can easily lead to additional unwanted harmonics that ultimately compromises the use of spectrum. Thus, in this paper, we focus on cancelling or suppressing harmonics in frequency-

shifted backscatter systems. Here, the term 'frequency-shifted' does not mean 'frequency modulation (FM) or frequency shifted keying (FSK) modulation'. It refers to the backscatter schemes whose operation bands are shifted away from the incoming RF carrier frequency, and the backscatter signal modulations can be diverse, e.g. FSK, Chirp Spread Spectrum (CSS) modulation in [23] and differential binary & quadrature phase-shift keying (DBPSK & DQPSK) modulations in [27] [28].

The basic operation of the backscatter frequency shifting is illustrated in Fig. 1, which is achieved by alternately toggling between two loads connected to the tag antenna with a frequency that matches the desired frequency shift, see f_{bs} in Fig. 1. Based on this operation,

- when more than one backscatter tones are synthesized, the FSK modulation can be obtained [29];
- when f_{bs} is not constant, but increases or decreases linearly with time, the CSS modulation can be obtained [23];
- when the square switching function is shifted in time with the step of a half (or a quarter) of the period, the DBPSK (or DQPSK) modulation can be obtained [27] [28].

In order to maximize the power of the backscatter signals, ideally the two loads Z_1 and Z_2 in Fig. 1 should be oppositely located on the outmost reflection coefficient circle in the Smith Chart, making open and short termination an obvious choice.
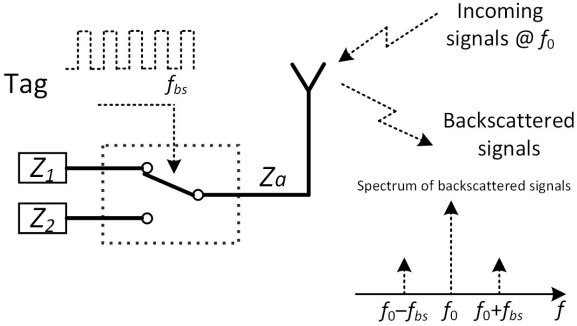

Fig. 1. Illustration of the basic operation of backscatter frequency shifting.

In order to facilitate the discussion later in this paper, the frequency shifted backscattering process is now mathematically elaborated.

It is assumed that the incoming electromagnetic wave is a one-tone signal S_{in} with a frequency of f_0, see (1).

$$S_{in} = \cos(2\pi f_0 t) \qquad (1)$$

Here the magnitude is normalized to unity, and the initial phase is set to be 0. When the switch, seen in Fig. 1, is toggling between open and short at a constant frequency of f_{bs}, the resulting reflection coefficient Γ_{bs} at the interface between the tag antenna and the loads can be represented as a square wave shown in Fig. 2.
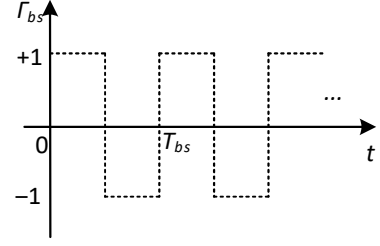

Fig. 2. The reflection coefficient Γ_{bs} in time when the switch is toggling between open and short at a frequency of $f_{bs} = 1/T_{bs}$.

The reflection coefficient Γ_{bs} in Fig. 2 can be Fourier expanded into a series of sine terms in (2),

$$\Gamma_{bs}(t) = \frac{4}{\pi} \sum_{n=1,3,5}^{\infty} \frac{1}{n} \sin(2n\pi f_{bs}t), \qquad (2)$$

from which, the backscatter signal S_{bs} can be obtained,

$$S_{bs} = S_{in} \cdot \Gamma_{bs}(t) = \frac{4}{\pi} \sum_{n=1,3,5}^{\infty} \frac{1}{n} \cos(2\pi f_0 t) \cdot \sin(2n\pi f_{bs}t). \quad (3)$$

Since $\cos(x) \cdot \sin(y) = 0.5 \times [\sin(x+y) - \sin(x-y)]$, the backscatter signal S_{bs} in (3) contains undesired first order mirror harmonic, e.g. at the frequency of $f_0 - f_{bs}$ (assuming $f_0 + f_{bs}$ is the desired frequency component), and higher order harmonics at the frequencies of $f_0 \pm nf_{bs}$ ($n = 3, 5, \dots$). It is also observed in (3) that the frequency conversion loss, namely the power loss when translating the incoming signal at f_0 to the desired backscatter signal at $f_0 + f_{bs}$, is $-20 \times \log_{10}(4/\pi \times 0.5) = 3.9$ dB. The unwanted mirror harmonic contains equivalent power levels while higher order harmonics are $-20 \times \log_{10}(1/n)$ dB lower when compared with the first harmonic, saying 9.5 dB and 14 dB lower for the 3rd and the 5th harmonics.

III. Harmonic Suppression with Load Impedances of Complex-values

Let us start from an ideal case of a backscatter tag that is able to synthesize reflection coefficient values, Γ_{bs1}, that on the Smith Chart can write a complete circle of magnitude 1. When the tag antenna load impedance is varied counterclockwise along this circle at a constant phase speed ω_1, the backscatter signal S_{bs1} becomes

$$S_{bs1} = \cos(2\pi f_0 t + \omega_1 t) = \cos[2\pi(f_0 + f_1)t], \qquad (4)$$

where $f_1 = \omega_1/(2\pi)$, and the incoming signal S_{in} in (1) is assumed.

This process can be mathematically expressed as

$$S_{bs1} = \mathrm{Re}\left(e^{j2\pi f_0 t} \cdot \Gamma_{bs1}\right), \qquad (5)$$

where

$$\Gamma_{bs1} = e^{j2\pi f_1 t}. \qquad (6)$$

From (4) it can be seen that in this ideal scenario, no harmonics are generated. It is also noted that when the reflection coefficient rotates clockwise at the phase speed ω_1, a pure backscatter tone at $f_0 - f_1$ can be obtained instead. However, constructing a backscatter tag that can synthesize a continuous reflection coefficient circle as in (6) can be problematic. Possible practical architectures can be a Single-Pole N-Throw switch connecting to N variable reactance loads (e.g. varactors or transistors), each covering a subsection of the required reflection coefficient circle, or the IQ backscatter module that can span a square area of the achievable impedance in Smith Chart [30]. These solutions are far from ideal as the loss associated with the active components would significantly shrink the magnitude of the reflection circle, which in turn compromise the link budget. Thus, in the remaining part of this section we investigate the effect when the Γ_{bs1} in (6) is discretized into M equal-spaced (in Smith Chart) complex impedance, see Γ_{bs2} in (7)

$$\Gamma_{bs2} = \begin{cases} e^{j0} & t \in \left[\frac{k}{f_1}, \frac{kM+1}{Mf_1} \right) \\ e^{j\frac{2\pi}{M}} & t \in \left[\frac{kM+1}{Mf_1}, \frac{kM+2}{Mf_1} \right) \\ \vdots \\ e^{j\frac{(M-1)\pi}{M}} & t \in \left[\frac{kM+M-1}{Mf_1}, \frac{k+1}{f_1} \right) \end{cases}, \qquad (7)$$

where $k = (0, 1, \ldots)$ and $M \geq 2$.

Using complex Fourier series expansion, $\Gamma_{bs2}(t)$ can be express as

$$\Gamma_{bs2}(t) = f_1 \sum_{p=-\infty}^{\infty} X_p \cdot e^{j2\pi p f_1 t}, \qquad (8)$$

where the coefficient X_p ($p = -\infty, \ldots, +\infty$) of the pth term of the Fourier expansion of the quantized reflection coefficient Γ_{bs2} in (7) can be calculated as in (9).

$$X_p = \int_0^{1/f_1} \Gamma_{bs2}(t) \cdot e^{-j2\pi p f_1 t} dt \qquad (9)$$

Substituting Γ_{bs2} in (7) into (9), after derivation we get

$$X_0 = 0, \qquad (10)$$

$$X_p \big|_{p \neq 0} = \frac{j}{2 p f_1 \pi} \sum_{m=0}^{M-1} \left(e^{j\frac{2\pi[m-p(m-1)]}{M}} - e^{j\frac{2\pi m(1-p)}{M}} \right). \qquad (11)$$

The magnitude of the pth term in (8), namely the magnitude of the backscattered signal at $f_0 + p f_1$, is

$$A_p = f_1 |X_p|, \qquad (12)$$

which, in dB, is listed in Table I. Here operator '$|\cdot|$' returns the absolute value of the enclosed term. It can be seen that the power of the desired first upper band harmonic converges to 0 dB when increasing M to infinity. This is the ideal case described by (5). For the other extreme case, when M is chosen to be 2, there are only two discrete load impedances (open and short), and it becomes the conventional case illustrated in Fig. 2 and described in (2) and (3). As expected, for $M = 2$, the 3rd (and the 5th) harmonic is 9.5 dB (and 14 dB) lower than the first upper band harmonic, consistent with the analysis performed in Section II. This table can be utilized to guide the system designs, such as the selection of parameters f_1 and M in order to suppress harmonics that cause detrimental inference to other users within the network.

TABLE I
NORMALIZED POWER (A_p IN DB) OF BACKSCATTER HARMONICS (UP TO $\pm$ 6) FOR DIFFERENT NUMBERS OF DISCRETE IMPEDANCES

p	M							
	2	3	4	5	6	7	8	9
−6	−∞	−∞	−∞	−∞	−∞	−15.9	−∞	−∞
−5	−17.9	−15.6	−∞	−∞	−14.4	−∞	−∞	−∞
−4	−∞	−∞	−∞	−12.6	−∞	−∞	−∞	−∞
−3	−13.4	−∞	−10.5	−∞	−∞	−∞	−∞	−∞
−2	−∞	−7.7	−∞	−∞	−∞	−∞	−∞	−∞
−1	−3.9	−∞	−∞	−∞	−∞	−∞	−∞	−∞
1	−3.9	−1.65	−0.91	−0.58	−0.40	−0.29	−0.22	−0.18
2	−∞	−∞	−∞	−∞	−∞	−∞	−∞	−∞
3	−13.4	−∞	−∞	−∞	−∞	−∞	−∞	−∞
4	−∞	−13.7	−∞	−∞	−∞	−∞	−∞	−∞
5	−17.9	−∞	−14.9	−∞	−∞	−∞	−∞	−∞
6	−∞	−∞	−∞	−16.1	−∞	−∞	−∞	−∞

In fact, the works in [26] and [23] focused on backscatter signal modulations, with a light touch on harmonic suppression. They found out that when the tag reflection coefficients are designed with 4-discrete [26] (and 8-discrete [23]) complex impedances the 1st mirror (and the 3rd and 5th) harmonics can be cancelled out. Clearly, these findings are the special cases shown in Table I, see the columns of $M = 4$ and 8. With the generic and systematic analysis provided in this section, it is realized that the backscatter signal waveforms with $M = 3$ and 7 should achieve similar harmonic suppression performance. These cannot be derived with the methods presented in [26] and [23].

IV. HIGHER-ORDER HARMONIC SUPPRESSION WITH LOAD IMPEDANCES OF REAL-VALUES

In the last section, we discussed the ideal frequency shifted backscatter system which generates no undesired harmonics. It is achieved with a continuous change of the tag antenna load impedance so that the reflection coefficient is moving along a circle centered at the perfectly matched

condition (i.e. center of the Smith Chart). This ideal scenario was further approximated by using only a limited number of discrete impedances of which most are complex, revealing a trade-off between harmonic suppression and the tag complexity. In this section we aim to further reduce the tag complexity by utilizing only real-valued reflection coefficients, which can be readily obtained using a single active component, such as a transistor [24]. The approaches of suppressing or cancelling higher order harmonics are now elaborated as below, leaving the treatment on mirror harmonics in Section V.

A. Continuous Real-valued Impedance

When the impedances of the tag loads can be continuously varied along the real axis on Smith Chart, a sine-shaped reflection coefficient in time can be synthesized as

$$\Gamma_{bs3} = \sin(2\pi f_1 t). \quad (13)$$

As a result, the backscatter signal S_{bs3} can be calculated as

$$S_{bs3} = \Gamma_{bs3} \cdot S_{in} = \sin(2\pi f_1 t) \cdot \cos(2\pi f_0 t)$$
$$= 0.5 \times \{\sin[2\pi(f_0+f_1)t] - \sin[2\pi(f_0-f_1)t]\}, \quad (14)$$

of which no higher order (larger than one) harmonics exist.

B. Discrete Real-valued Impedance

When the impedances of the tag loads can only be selected from a limited number of discrete real values, only a subsets of higher order harmonics can be suppressed or cancelled out.

Recalling the backscatter signal in (3) generated by the two-state real-valued square reflection coefficient, the higher order harmonic components are extracted and expressed in (15).

$$S_{bs}^{(n)}\Big|_{n=3,5,\dots} = \frac{2B}{n\pi}\left\{\sin\left[2\pi\left(f_0+nf_{bs}\right)t\right] - \sin\left[2\pi\left(f_0-nf_{bs}\right)t\right]\right\} \quad (15)$$

Here, B, the magnitude of the square reflection coefficient seen in Fig. 3, is added to facilitate the later discussion in this paper.

When it is preferred in a network to eliminate the third ($n = 3$) harmonics, we can synthesize another square-shaped reflection coefficient Γ_{bs4} with a frequency of $f_{bs4} = 3f_{bs}$, see the dashed curve in Fig. 3. The first harmonics associated with this newly generated Γ_{bs4} can be derived as

$$S_{bs4}^{(1)} = \frac{2C}{\pi}\left\{\sin\left[2\pi\left(f_0+f_{bs4}\right)t\right] - \sin\left[2\pi\left(f_0-f_{bs4}\right)t\right]\right\}$$
$$= \frac{2C}{\pi}\left\{\sin\left[2\pi\left(f_0+3f_{bs}\right)t\right] - \sin\left[2\pi\left(f_0-3f_{bs}\right)t\right]\right\}, \quad (16)$$
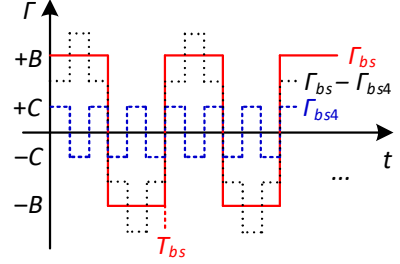
where C is the magnitude of Γ_{bs4}.

Fig. 3. Discrete real-valued reflection coefficients for third harmonic cancellation.

Comparing (16) and the third harmonics ($n = 3$) in (15), it can be seen that when $C = B/3$, the first harmonics associated with the Γ_{bs4} and the third harmonics associated with Γ_{bs} are identical. This indicates that the combined reflection coefficient ($\Gamma_{bs} - \Gamma_{bs4}$) generates no unwanted frequency components at $f_0 \pm 3f_{bs}$. The resulting four-state discrete reflection coefficient ($\Gamma_{bs} - \Gamma_{bs4}$) is plotted also in Fig. 3 (the dotted line). In a two-state square waveform case, see Fig. 2, the maximum magnitude of the reflection coefficient is 1, which results in the first harmonics of –3.9 dB. While in the four-state case in Fig. 3, $B + C = 4B/3$ has to be less than 1, so that $B \leq 0.75$. This gives an additional 2.5 dB reduction to the first harmonics. Using the same approach, we can further cancel out other higher order harmonics, which would ultimately converge to the continuous real-valued case discussed in Subsection A earlier that has the first harmonics of –6 dB. In practice, according to the system and network requirements, we can selectively eliminate (or suppress down below a defined threshold) the harmonics that present in the allocated frequency bands for other users.

V. MIRROR HARMONIC SUPPRESSION WITH ORTHOGONAL LOADS

In Table I, it can be observed that when $M > 2$ there is no first order mirror ($p = -1$) harmonic, but the harmonics of the orders ($1 - M$) and ($1 + M$) are present. In this section, we explore a different approach and hardware architecture to remove all mirror harmonics.

From the trigonometric identities shown in (17) and (18), it is realized that if a 90° shifted copy of the incoming signal S_{in} in (1) and 90° shifted copies of all terms in (2) can be created, namely $\cos(2\pi f_0 t + \pi/2)$ and $\sin(2n\pi f_{bs}t + \pi/2)$, all the mirror harmonics, i.e. at ($f_0 - nf_{bs}$), can be cancelled out.

$$\cos(x)\cdot\sin(y) = 0.5\times[\sin(x+y) - \sin(x-y)] \quad (17)$$

$$\sin(x)\cdot\cos(y) = 0.5\times[\sin(x+y) + \sin(x-y)] \quad (18)$$

The 90° shifted S_{in} can be readily obtained by adding a quarter wavelength. Whereas in order to generate 90° phase shifted copies of all the terms in (2), we move the square

waveform Γ_{bs} in Fig. 2 leftwards by $T_{bs}/4$, i.e. replacing t by $t + T_{bs}/4$ in (2). All these operations can be performed using the IQ backscatter modulator described in [14] [18], which is shown in Fig. 4. Here, the incoming signal S_{in} is first equally power split before being phase delayed by 45° in the top branch. As the signal will experience this phase delay twice, the total phase shift of the $0.707 \times S_{in}$ in the top branch becomes the required 90°. To facilitate readers' understanding, the signal flows are labelled in Fig. 4. The backscattered signal S_{bs5} can be expressed as

$$S_{bs5} = 0.5\Gamma_Q \cdot \cos(2\pi f_0 t) - 0.5\Gamma_I \cdot \sin(2\pi f_0 t), \quad (19)$$

where Γ_I and Γ_Q are the reflection coefficients of the two transistors, controlled by the gate voltage V_I and V_Q in Fig. 4. As discussed earlier, Γ_I is designed to be a quarter time period shifted when compared with Γ_Q. They can be Fourier expanded and are written in (20) and (21).

$$\Gamma_I(t) = -\frac{4}{\pi} \sum_{n=1,3,5}^{\infty} \frac{1}{n} \cos(2n\pi f_{bs}t) \quad (20)$$

$$\Gamma_Q(t) = \frac{4}{\pi} \sum_{n=1,3,5}^{\infty} \frac{1}{n} \sin(2n\pi f_{bs}t) \quad (21)$$
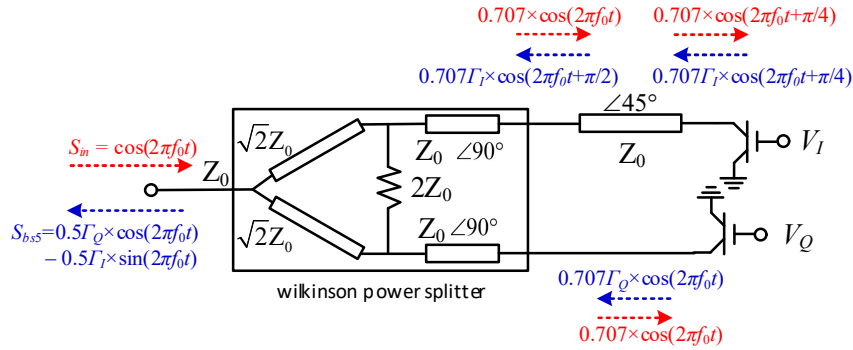
Substituting (20) and (21) into (19), we get

$$S_{bs5} = \frac{2}{\pi} \sum_{n=1,3,5}^{\infty} \frac{1}{n} \cos(2\pi f_0 t) \cdot \sin(2n\pi f_{bs}t)$$

$$+ \frac{2}{\pi} \sum_{n=1,3,5}^{\infty} \frac{1}{n} \sin(2\pi f_0 t) \cdot \cos(2n\pi f_{bs}t)$$

$$= \frac{2}{\pi} \sum_{n=1,3,5}^{\infty} \frac{1}{n} \sin\left[2\pi(f_0 + nf_{bs})t\right] \quad . \quad (22)$$

It can be seen from (22) that all the lower-band mirror harmonics are removed.

Similar to the analysis in Section IV, the nth ($n \geq 3$) higher order upper-band harmonic can be further eliminated by creating another pair of Γ_I and Γ_Q that are square waveforms with a frequency of nf_{bs}. For example, the first Fourier expansion terms of the Γ_{I1} and Γ_{Q1} in Fig. 5 are identical to the third Fourier expansion terms of the Γ_I and Γ_Q, wherein $C = B/3$. As a consequence, in the IQ backscatter modulator, when the 4-state discrete reflection coefficients $(\Gamma_I - \Gamma_{I1})$ and $(\Gamma_Q - \Gamma_{Q1})$, seen in Fig. 5, are synthesized by the two transistors in the two branches, the harmonic at $f_0 + 3f_{bs}$ is removed. Again, since the magnitude of the reflection coefficient is upper bounded by 1, a 2.5 dB loss is introduced to the desired frequency component at $f_0 + f_{bs}$.

Fig. 4. IQ backscatter modulator enabled mirror harmonic cancellation.

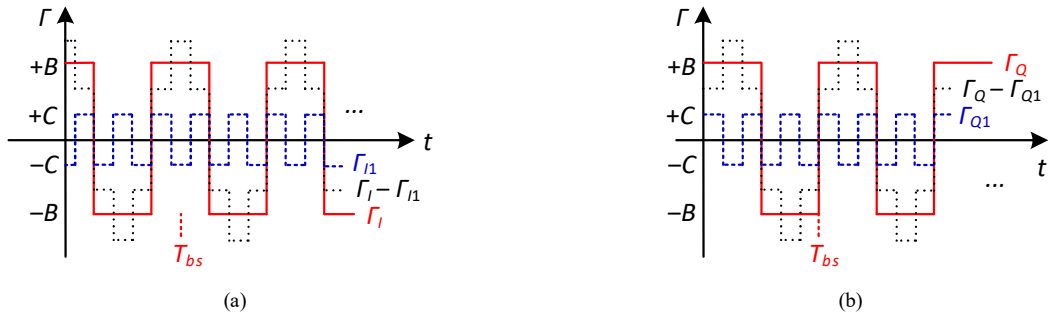(a)   (b)

Fig. 5. Reflection coefficients at I and Q paths required to remove lower-band harmonics and the third upper-band harmonic.

VI. Exemplar Systems

Various harmonic suppression approaches in the frequency shifted backscatter links are presented in Sections III, IV and V. It is worth noting that the authors do not intend to compare these methods, as different frequency allocations of backscatter users and tag hardware constraints require a bespoke combination of harmonic suppression solutions in the network. This aspect is now presented using a series of examples.

Prerequisites: An example backscatter network comprises up to 4 backscatter nodes, all of which performing 2FSK modulation. Here it is assumed that the frequency shifts (relative to the incoming RF carrier frequency at f_0) of the two tones in the 2FSK signals for each user are $f_{1\_user\{1,2,3,4\}} = \{1,-1,3,5\}$ kHz and $f_{2\_user\{1,2,3,4\}} = \{2,-2,4,6\}$ kHz. The 2FSK symbol periods for all users are chosen as 2 ms, which guarantees the orthogonality of the two sinc-function shaped tones in the frequency domain [31]. Both Time Division Multiple Access (TDMA) and Frequency Division Multiple Access (FDMA) schemes, as well as their combinations, can be adopted to coordinate multiple user links. The harmonic suppression methods proposed in the previous sections are useful when multiple users are required to be accommodated in a shared time slot. The 4 subsections below are now investigating the scenarios where different numbers of users are operating simultaneously in this example backscatter network.

A. Single-user 2FSK Modulated Backscatter Link

In this subsection, the performance of a single-user (i.e. User1) 2FSK modulated backscatter link is presented via simulated bit error rates (BERs). This is acted as the benchmark for the multi-user backscatter networks that will be discussed in the following subsections.
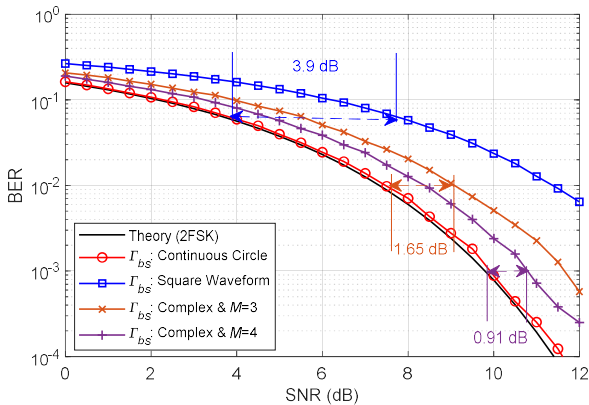

Fig. 6. Simulated BER results of the single-user 2FSK modulated backscatter links. The cases of ideal continuous reflection coefficient circle in (2), and the discrete complex reflection coefficients with $M = 2, 3, 4$ (see (7) and Table I) are assumed, respectively. (When $M = 2$, it is the case of the square reflection coefficient waveform plotted in Fig. 2.)

From the BER simulation results in Fig. 6, it can be seen that as expected the case of the ideal continuous reflection coefficient circle described in (2) gives the 2FSK

modulated backscatter link the same performance as the theoretical 2FSK link because no backscatter energy is wasted via harmonics. While in practice, the performance is commonly traded off with the significant reduction of the tag circuitry complexity, i.e. using a limited number of discrete load impedances instead of the continuous varied impedances. These simplified tags require extra signal to noise ratio (SNR) of values shown in both Table I and Fig. 6 to achieve the same BER performance in the ideal 2FSK link. Here, the SNR is defined as the ratio of received signal power, including desired and all undesired harmonics, and the system/channel noise power.

B. Two 2FSK Modulated Backscatter Users

When the User1 and User2, who occupy mirror symmetric frequency bands relative to f_0, are required to operate simultaneously, the 1st and 2nd mirror harmonics of both users cannot present. It is noted that the 2nd mirror harmonic of $f_{1\_user\{1,2\}}$ falls into the band of $f_{2\_user\{2,1\}}$ in this example. As evidenced in Fig. 7, without the treatment of harmonics when both User1 and User2 adopt square waveform reflection coefficients, neither of the user links work. From Table I, it can bee seen that when $M \geq 4$, no 1st and 2nd mirror harmonics exist. In addition, as discussed in Section V the IQ backscatter modulator is able to suppress all mirror harmonics. Hence, both these two approaches are capable of eliminating inter-user (User1 and User2) interference, the BER performance of which is plotted also in Fig. 7. It is noted that the IQ backscatter modulator-enabled mirror harmonic suppression tag achieves the same performance as that in the conventional square waveform-based backscatter tag.
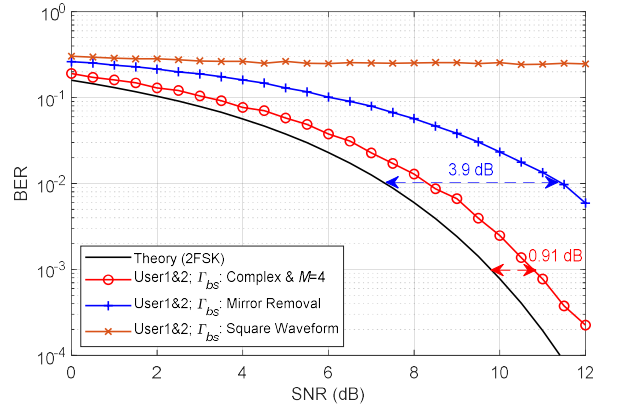

Fig. 7. Simulated BER results of the backscatter network comprising two, i.e. User1 and User2, 2FSK modulated links operating simultaneously.

When the User1 and User3, who occupy consecutive frequency bands on the same side relative to f_0, are required to operate simultaneously, the 3rd and 4th harmonics (and the 2nd harmonic) of f_{1_user1} (and f_{2_user1}) fall into the frequency band of User3. As a consequence, all the 2nd, 3rd and 4th harmonics for User1 should be avoided. On the other hand, no harmonics of User3 will affect the operation of User1.

As can be seen in Fig. 8, when both users perform square

waveform based 2FSK backscatter modulation, i.e. the Case1, User1's performance is unaffected, whereas the User3's performance is slightly degraded due to the 3rd harmonic interference of $(-13.4+3.9) = -9.5$ dB caused by f_{1_user1}, seen in Table I. Other approaches, like the discrete ($M = 4$) complex Γ_{bs} (Case2), the continuous real-valued Γ_{bs} (Case3), and discrete (with the 3rd harmonics removed) real-valued Γ_{bs} (Case4), are able to avoid inter-user interference. However, only the Case2 has better performance compared with that in the Case1.
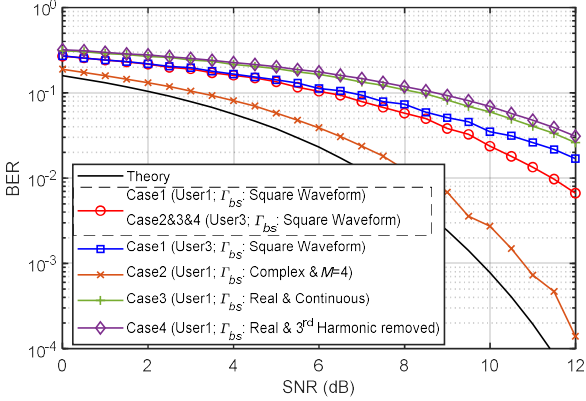

Fig. 8. Simulated BER results of the backscatter network comprising two, i.e. User1 and User3, 2FSK modulated links operating simultaneously.

C. Three 2FSK Modulated Backscatter Users

When the User1, User2 and User3 operate in a same time slot, the User1 and User2 will severely interfere each other and they will degrade the performance of the User3 if no harmonic control is applied, see Case1 (conventional square waveform based Γ_{bs} for all users) in Fig. 9. Since the frequency band of the User1 locates on the same side (relative to f_0) with that of the User3, while the frequency band of the User2 is on the opposite side, different harmonic suppression strategies are required. For Case2 in Fig. 9, it can be observed that when the User1 is designed based on the discrete ($M = 4$) complex Γ_{bs}, and the mirror
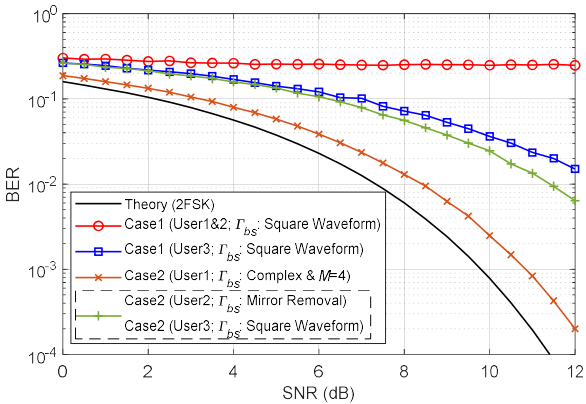

Fig. 9. Simulated BER results of the backscatter network comprising three, i.e. User1, User2 and User3, 2FSK modulated links operating simultaneously.

harmonics are removed for the User2, no inter-user interference exist. There is no constraint on the User3. In the Case2 example, it is assumed that the User3 adopts the conventional square waveform based 2FSK design.

D. More 2FSK Modulated Backscatter Users

Some typical harmonic suppression strategies and their applicability are illustrated in the previous subsections. When more users are configured to backscatter simultaneously, the similar harmonic planning approaches can be exploited, subject to the constraints on the tag circuitry architecture and power budgets. It is noted that higher order harmonics tends to have limited interference effects as the power is generally low. In Fig. 10, the BER simulations of a 4-user example for two configuration scenarios are presented. There can be plenty of combinations with the trade-off adjusted among BER performance for each individual users and their tag complexity.
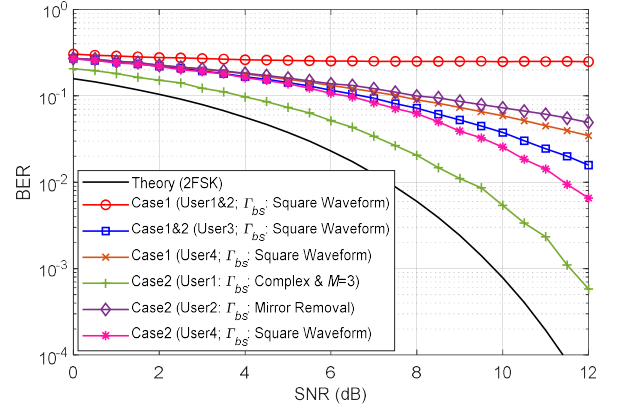

Fig. 10. Simulated BER results of the backscatter network comprising four, i.e. User1, User2, User3, and User4, 2FSK modulated links operating simultaneously.

VII. CONCLUSION

It is the first time that the harmonics in the frequency shifted backscatter communications have been systematically investigated. This study has revealed several tradeoffs between the system complexity, i.e. the requirements on tag antenna reflection coefficients, and the harmonic suppression performance. Importantly, this paper proposed approaches to independently manipulate mirror harmonics and higher order harmonics. The effectiveness of the various methods has been demonstrated using an example multi-user backscatter network. This paper can serve as a guideline for network engineers to optimize the spectrum usage and efficiency in large-scale backscatter networks. The laboratory and field measurement campaign will be conducted to validate the various proposed approaches in this paper.

REFERENCES

[1] W. Saad, M. Bennis, and M. Chen, "A vision of 6G wireless Systems: applications, trends, technologies, and open research problems," *IEEE Network*, in press.

[2] M. Dixit, J. Kumar, and R. Kumar, "Internet of things and its challenges," in *Int. Conf. Green Computing Internet of Things (ICGCIoT)*, Noida, India, Oct. 2015, pp. 810–814.

[3] F. Alimenti, V. Palazzi, C. Mariotti, P. Mezzanotte, R. Correia, N. B. Carvalho, and L. Roselli, "Smart hardware for smart objects: microwave electronic circuits to make objects smart," *IEEE Microw. Mag.*, vol. 19, no. 6, pp. 48–68, Sept. - Oct. 2018.

[4] M. L. Memon, N. Saxena, A. Roy, and D. R. Shin, "Backscatter communications: Inception of the battery-free era—A comprehensive survey," *Electron.*, vol. 8, no., 2, Jan. 2019.

[5] D. Belo, D. Ribeiro, P. Pinho, and N. B. Carvalho, "A selective, tracking, and power adaptive far-field wireless power transfer system," *IEEE Trans. Microw. Theory Tech.*, vol. 67, no. 9, pp. 3856–3866, Sept. 2019.

[6] K. W. Choi, S. Hwang, A. A. Aziz, H. H. Jang, J. S. Kim, D. S. Kang, and D. I. Kim, "Simultaneous wireless information and power transfer (SWIPT) for Internet of Things: Novel receiver design and experimental validation," *IEEE Internet of Things J.*, vol. 7, no. 4, pp. 2996–3012, Apr. 2020.

[7] H. J. Visser and R. J. M. Vullers, "RF energy harvesting and transport for wireless sensor network applications: Principles and requirements," *Proc. IEEE*, vol. 101, no. 6, pp. 1410–1423, June 2013.

[8] C. Song, Y. Huang, J. Zhou, J. Zhang, S. Yuan, and P. Carter, "A high-efficiency broadband rectenna for ambient wireless energy harvesting," *IEEE Trans. Antennas Propag.*, vol. 63, no. 8, pp. 3486–3495, Aug. 2015.

[9] A. Liu, M. Shahzad, X. Liu, and K. Li, *RFID Protocol Design, Optimization, and Security for the Internet of Things*. IET book, 2017. ISBN 978-1-78561-332-6.

[10] R. Smith, Y. Ding, G. Goussetis, and M. Dragone, "A COTS (UHF) RFID floor for device-free ambient assisted living monitoring," in *Int. Symp. Ambient Intelligence (ISAmI 2020)*, L'Aquila, Italy, 2020.

[11] J. M. Kahn, R. H. Katz and K. S. J. Pister, "Emerging challenges: Mobile networking for "Smart Dust"," *J. Commun. Networks*, vol. 2, no. 3, pp. 188–196, Sept. 2000.

[12] G. Vougioukas, S. N. Daskalakis, and A. Bletsas, "Could battery-less scatter radio tags achieve 270-meter range?" in *Proc. IEEE Wireless Power Transfer Conf. (WPTC)*, Aveiro, Portugal, May 2016, pp. 1–3.

[13] A. Varshney, C. Pérez-Penichet, C. Rohner, and T. Voigt, "LoRea: A backscatter architecture that achieves a long communication range," in *Proc. ACM Embedded Netw. Sensor Syst. (SenSys)*, Delft, Netherlands, Nov. 2017, pp. 1–14.

[14] D. Belo, R. Correia, Y. Ding, S. Daskalakis, G. Goussetis, A. Georgiadis, and N. Carvalho, "IQ impedance modulator front-end for low-power LoRa backscattering devices," *IEEE Trans. Microw. Theory Tech.*, vol. 67, no. 12, pp. 5307–5314, Dec. 2019.

[15] J. Hester and M. Tentzeris, "Inkjet-printed flexible mm-Wave Van-Atta reflectarrays: A solution for ultralong-range dense multitag and multisensing chipless RFID implementations for IoT smart skins," *IEEE Trans. Microw. Theory Tech.*, vol. 64, no. 12, pp. 4763–4773, Dec. 2016.

[16] F. Amato, C. W. Peterson, B. P. Degnan, and G. D. Durgin, "Tunneling RFID tags for long-range and low-power microwave applications," *IEEE J. Radio Frequency Identification*, vol. 2, no. 2, pp. 93–103, June 2018,

[17] S. J. Thomas and M. S. Reynolds, "A 96 Mbit/sec, 15.5 pJ/bit 16-QAM modulator for UHF backscatter communication," in *Proc. IEEE Int. Conf. RFID*, Apr. 2012, pp. 185–190.

[18] R. Correia, A. Boaventura, and N. B. Carvalho, "Quadrature amplitude backscatter modulator for passive wireless sensors in IoT applications," *IEEE Trans. Microw. Theory Tech.*, vol. 65, no. 4, pp. 1103–1110, Feb. 2017.

[19] Y. Ding, G. Goussetis, R. Correia, R. Lihakanga, N. Carvalho, and P. Petridis, "Enabling multicarrier backscattering communications," in *IEEE MTT-S Int. Wirless Symp.*, Shanghai, China, 2020.

[20] B. Kellogg, A. Parks, S. Gollakota, J. R. Smith, and D. Wetherall, "Wi-Fi backscatter: Internet connectivity for RF-powered devices," in *Proc. ACM SIGCOMM*, Chicago, IL, USA, Jun. 2014, pp. 1–12.

[21] S. N. Daskalakis, R. Correia, G. Goussetis, M. M. Tentzeris, N. B. Carvalho and A. Georgiadis, "4-PAM modulation of ambient FM backscattering for spectrally efficient low power applications," *IEEE Trans. Microw. Theory Tech.*, vol. 66, no. 12, pp. 5909–5921, Dec. 2018.

[22] R. Correia and N. B. Carvalho, "Design of high order modulation backscatter wireless sensor for passive IoT solutions," in *Proc. IEEE Wireless Power Transfer Conf. (WPTC)*, Aveiro, Portugal, 2016, pp. 1–3.

[23] V. Talla, M. Hessar, B. Kellogg, A. Najafi, J. Smith, and S. Gollakota, "LoRa backscatter: Enabling the vision of ubiquitous connectivity," *Proc. ACM Interact. Mobile Wearable Ubiquitous Technol.*, vol. 1, no. 3, Sep. 2017.

[24] J. Kimionis and M. M. Tentzeris, "Pulse shaping: The missing piece of backscatter radio and RFID," *IEEE Trans. Microw. Theory Tech.*, vol. 64, no. 12, pp. 4774–4788, Dec. 2016.

[25] J. F. Ensworth and M. S. Reynolds, "Every smart phone is a backscatter reader: Modulated backscatter compatibility with Bluetooth 4.0 Low Energy (BLE) devices," in *Proc. IEEE Int. Conf. RFID*, San Diego, CA, 2015, pp. 78–85.

[26] V. Iyer, V. Talla, B. Kellogg, S. Gollakota, and J. Smith, "Inter-technology backscatter: Towards Internet connectivity for implanted devices," in *Proc. ACM SIGCOMM Conf. (SIGCOMM'16)*, New York, USA, Aug. 2016, pp. 356–369.

[27] B. Kellogg, V. Talla, S. Gollakota, and J. R. Smith, "Passive Wi-Fi: Bringing low power to Wi-Fi transmissions," in *Proc. USENIX Symp. Netw. Syst. Design Implement. (NSDI)*, Santa Clara, CA, USA, Mar. 2016, pp. 151–164.

[28] G. Yang, Y. Liang, R. Zhang, and Y. Pei, "Modulation in the air: Backscatter communication over ambient OFDM carrier," *IEEE Trans. Commun.*, vol. 66, no. 3, pp. 1219–1233, Mar. 2018.

[29] V. Liu, A. Parks, V. Talla, S. Gollakota, D. Wetherall, and J. R. Smith, "Ambient backscatter: wireless communication out of thin air," *ACM SIGCOMM Comput. Commun. Rev.*, vol. 43, no. 4, pp. 39–50, Oct. 2013.

[30] R. Correia, Y. Ding, S. Daskalakis, P. Petridis, G. Goussetis, A, Georgiadis, and N. Carvalho, "Chirp based backscatter modulation," in *Int. Microw. Symp. 2019*, Boston, Massachusetts, US, Jun. 2–7, 2019.

[31] W. Ismail, J. S. Mandeep, E. Hamza, and H. S. Hamid, "Analyze BER performance of wireless FSK system," *Microwaves and RF*, vol. 48, 2009.
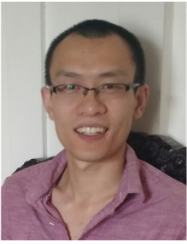
YUAN DING (M'19) received his Bachelor's degree from Beihang University (BUAA), Beijing, China, in 2004, received his Master's degree from Tsinghua University, Beijing, China, in 2007, and received his Ph.D. degree from Queen's University of Belfast, Belfast, UK, in 2014, all in Electronic Engineering.

He was a radio frequency (RF) Engineer in Motorola R&D Centre (Beijing, China) from 2007 to 2009, before joining Freescale Semiconductor Inc. (Beijing, China) as an RF Field Application Engineer, responsible for high power base-station amplifier design, from 2009 to 2011. He is now an Assistant Professor at the Institute of Sensors, Signals and Systems (ISSS) in Heriot-Watt University, Edinburgh, UK. His research interests are in antenna array, physical layer security, and 5G related areas.

Dr. Ding was the recipient of the IET Best Student Paper Award at LAPC 2013 and the recipient of the Young Scientists Awards in General Assembly and Scientific Symposium (GASS), 2014 XXXIst URSI.

ROMWALD LIHAKANGA received his Bachelor's degree in electronics and telecommunications engineering from Dar es Salaam Institute of Technology (DIT) Dar es salaam, Tanzania, in 2009, received his Master's degree in Electronic Product design from Glamorgan University, Wales, UK, in 2012, currently working on his Ph.D. degree in Civil and Electronic Engineering in Heriot Watt University, UK.

He is also an Assistant Lecturer with the Department of Electronics and Telecommunication, Dar es salaam Institute of Technology, Tanzania. His current research interests include embedded systems design, wireless power transfer and RF backscattering, sensors/sensor interface circuits, and wireless sensors for SHM applications.

RICARDO CORREIA (GS'15) received the M.Sc. degree in electronics and telecommunications engineering and the Ph.D. degree in electrical engineering from the University of Aveiro, Aveiro, Portugal, in 2009 and 2019, respectively.

He was an Automation and Electrical Engineer and a Researcher of embedded systems and signal processing. He is currently a Researcher with Sinuta SA., Aveiro, where he focuses on transmission and reception systems of electronically oriented signals for next-generation satellite constellations. He is also a collaborator with the Institute of Telecommunications, University of Aveiro. His current research interests include wireless power transfer, energy harvesting, wireless passive sensors for space applications, and low power communications.

Dr. Correia is a member of the IEEE Microwave Theory and Techniques Society. He was a recipient of the 2016 URSI/ANACOM Prize awarded by the URSI Portuguese Section and Portuguese National Authority of Communications. He is also a Reviewer for IET Microwaves, Antennas and Propagation, Wireless Power Transfer, and the IEEE Transactions on Microwave Theory and Techniques.
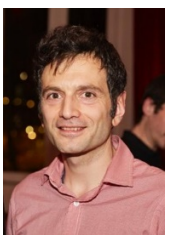
GEORGE GOUSSETIS (S'99, M'02, SM'12) received the Diploma degree in Electrical and Computer Engineering from the National Technical University of Athens, Greece, in 1998, and the Ph.D. degree from the University of Westminster, London, UK, in 2002. In 2002 he also graduated B.Sc. in physics (first class) from University College London (UCL), UK.

In 1998, he joined the Space Engineering, Rome, Italy, as RF Engineer and in 1999 the Wireless Communications Research Group, University of Westminster, UK, as a Research Assistant. Between 2002 and 2006 he was a Senior Research Fellow at Loughborough University, UK. He was a Lecturer (Assistant Professor) with Heriot-Watt University, Edinburgh, UK between 2006 and 2009 and a Reader (Associate Professor) with Queen's University Belfast, UK, between 2009 and 2013. In 2013 he joined Heriot-Watt as a Reader and was promoted to Professor in 2014, where he currently directs the Institute of Sensors Signals and Systems. He has authored or co-authored over 500 peer-reviewed papers five book chapters one book and four patents. His research interests are in the area of microwave and antenna components and subsystems.

Dr. Goussetis has held a research fellowship from the Onassis foundation in 2001, a research fellowship from the UK Royal Academy of Engineering between 2006 to 2011 and European Marie-Curie experienced researcher fellowships in 2011-12 and again in 2014-17. He is the co-recipient of the 2011 European Space Agency young engineer of the year prize, the 2011 EuCAP best student paper prize, the 2012 EuCAP best antenna theory paper prize and the 2016 Bell Labs prize. He has served as Associate Editor to the IEEE Antennas and Wireless Propagation Letters.

Nuno Borges Carvalho (S'97–M'00–SM'05-F'15) was born in Luanda, Angola, in 1972. He received the Diploma and Doctoral degrees in electronics and telecommunications engineering from the University of Aveiro, Aveiro, Portugal, in 1995 and 2000, respectively.

He is currently a Full Professor and a Senior Research Scientist with the Institute of Telecommunications, University of Aveiro and an IEEE Fellow. He coauthored Intermodulation in Microwave and Wireless Circuits (Artech House, 2003), Microwave and Wireless Measurement Techniques (Cambridge University Press, 2013) and White Space Communication Technologies (Cambridge University Press, 2014). He has been a reviewer and author of over 200 papers in magazines and conferences. He is the Editor in Chief of the Cambridge Wireless Power Transfer Journal, an associate editor of the IEEE Microwave Magazine and former associate editor of the IEEE Transactions on Microwave Theory and Techniques and IET Microwaves Antennas and Propagation Journal.

He is the co-inventor of six patents. His main research interests include software-defined radio front-ends, wireless power transmission, nonlinear distortion analysis in microwave/wireless circuits and systems, and measurement of nonlinear phenomena. He has recently been involved in the design of dedicated radios and systems for newly emerging wireless technologies.

Prof. Borges Carvalho is a member of the IEEE MTT ADCOM, the past-chair of the IEEE Portuguese Section, MTT-20 and MTT-11 and also belong to the technical committees, MTT-24 and MTT-26. He is also the vice-chair of the URSI Commission A (Metrology Group). He was the recipient of the 1995 University of Aveiro and the Portuguese Engineering Association Prize for the best 1995 student at the University of Aveiro, the 1998 Student Paper Competition (Third Place) of the IEEE Microwave Theory and Techniques Society (IEEE MTT-S) International Microwave Symposium (IMS), and the 2000 IEE Measurement Prize.

He is a Distinguished Microwave Lecturer for the IEEE Microwave Theory and Techniques Society.